World Electric Vehicle Journal

MDPI

Article

Energy-Saving Optimization for Electric Vehicles in Car-Following Scenarios Based on Model Predictive Control

Yang Liu [1], Chuyang Yao [1], Cong Guo [1], Zhong Yang [2] and Chunyun Fu [1,*]

[1] College of Mechanical and Vehicle Engineering, Chongqing University, Chongqing 400044, China
[2] Chongqing Changan Automobile Co., Ltd., Chongqing 400023, China
* Correspondence: fuchunyun@cqu.edu.cn

Abstract: In this paper, an economy-oriented car-following control (EOCFC) strategy is proposed for electric vehicles in car-following scenarios. Specifically, a controller based on model predictive control (MPC) is developed to optimize the host vehicle's speed for better energy economy while ensuring good car-following performance and ride comfort. The vehicle's energy consumption is accurately quantified in the form of demand power, which is incorporated in the cost function for energy optimization. The proposed EOCFC strategy is evaluated using three standard test cycles, i.e., New European Driving Cycle (NEDC), Urban Dynamometer Driving Schedule (UDDS) and Worldwide Harmonized Light Vehicles Test Cycle (WLTC), in comparison with a typical multi-objective adaptive cruise control strategy. The evaluation results demonstrate that the proposed EOCFC improves the energy economy of the host vehicle by 0.53%, 3.33% and 1.51%, under the NEDC, UDDS and WLTC test cycles respectively.

Keywords: adaptive cruise control (ACC); car-following control; multi-objective optimization

Citation: Liu, Y.; Yao, C.; Guo, C.; Yang, Z.; Fu, C. Energy-Saving Optimization for Electric Vehicles in Car-Following Scenarios Based on Model Predictive Control. *World Electr. Veh. J.* **2023**, *14*, 42. https://doi.org/10.3390/wevj14020042

Academic Editor: Joeri Van Mierlo

Received: 29 December 2022
Revised: 22 January 2023
Accepted: 31 January 2023
Published: 5 February 2023

1. Introduction

1.1. Background

In recent years, the deterioration of the environment through pollution and energy shortage have imposed more stringent requirements on the energy consumption of road vehicles [1]. Compared with single-motor-drive electric vehicles (EVs), front-and-rear-independent-drive electric vehicles (FRIDEVs) can further exploit the energy-saving potential of EVs by means of appropriate torque distribution between the front and rear motors [2].

In addition to economical hardware configurations such as FRIDEVs, software such as eco-driving strategies also plays a crucial role in energy consumption reduction. It has been shown in the literature that by using eco-driving strategies [3–5], the energy consumption of vehicles can be effectively reduced. In recent years, advanced driving assistance systems (ADASs) have entered a new era of fast development and commercialization. Adaptive cruise control (ACC), as a typical type of ADAS, is an ideal carrier for eco-driving strategies to maximize their energy-saving potentials [6]. ACC assists the driver in achieving longitudinal control by adaptively adjusting the throttle or brake to maintain a certain cruise speed or to ensure an appropriate inter-vehicle distance, based on the state information of the preceding vehicle obtained by onboard sensors. Compared to human drivers who control longitudinal motions in an intuitive pattern, the longitudinal automation provided by ACC enables EVs to better execute eco-driving strategies [7], and as a result, the economy of EVs can be improved to a greater extent by designing an economy-oriented ACC system.

1.2. Literature Review

Economy-oriented ACC is originated from economy-oriented cruise control which improves vehicle economy by planning the economical cruise speed for the host vehicle [8].

Driven by the fast development of ACC systems, in recent years attention has been increasingly paid to energy-saving control in car-following scenarios [9]. Two main categories of car-following control strategies have been proposed in the literature to improve energy economy: rule-based strategies [10–14] and optimization-based strategies [15–21].

The rule-based strategies are mainly to achieve energy savings based on driving experience. Li et al. [10,11] proposed a PnG control strategy to minimize fuel consumption in car-following scenarios, which led to the reduction of fuel consumption by 20% compared to the LQ-based controller. Ioannou and Stefanovic [12] pointed out that the fuel economy of the host vehicle can be improved by smoothing its acceleration. Zhang and Ioannou [13] designed a proportional-integral (PI) controller for trucks to reduce fuel consumption by avoiding unnecessary acceleration and braking. Wu et al. [14] proposed a fuel economy optimization system in which the Lagrange multipliers method was used to calculate the desired acceleration or deceleration for fuel consumption optimization. However, the above rule-based strategies highly rely on human expertise and intuition, and as a result, the energy-saving potential of vehicles has not been fully exploited.

For optimization-based strategies, the control action is determined by optimizing a certain cost function which normally consists of one or more performance indicators. Li et al. [15] first proposed to utilize model predictive control (MPC) to achieve multi-objective optimization for better energy economy in car-following scenarios. Specifically, in their approach [15,16], the host vehicle's acceleration was used to characterize its energy consumption, and a cost function was designed by taking into account car-following error and fuel consumption. Additionally, the requirements for safety, car-following performance and longitudinal ride comfort were also incorporated in this optimization problem as constraints. Luo et al. [17] also employed acceleration as an indicator of energy consumption. However, in their approach, acceleration was not directly incorporated into the cost function; instead, it was controlled to track a pre-designed smooth curve. Schmied et al. [18] designed an MPC-based car-following controller, in which vehicle speed and acceleration were employed to measure static fuel consumption. Jia et al. [19,20] developed an economy-oriented ACC system based on MPC for EVs. This approach took into account the effect of surrounding traffic information on vehicle speed and planned optimal speed profile for the host vehicle, aiming to achieve car-following control with low energy consumption. Madhusudhanan et al. [21] proposed a control scheme suitable for signalized intersections. In this method, to reduce energy consumption of the host vehicle, its speed was regulated according to future traffic signals and states of the preceding vehicle. In the above studies, energy economy was optimized by means of acceleration smoothing. However, acceleration is only an indirect measure (or indicator) of energy consumption, and it cannot accurately quantify energy consumption of the host vehicle. As a result, control strategies based on acceleration regulation may not lead to optimal economy performance.

To fully explore the energy-saving potential of EVs, an economy-oriented car-following control (EOCFC) scheme is proposed in this paper. For the host vehicle, three types of control objectives (i.e., car-following performance, ride comfort and energy economy) are taken into consideration in the controller design, and the demand power of the host vehicle is employed as an indicator to reflect its energy consumption. Then, a cost function which incorporates the above three objectives is constructed and solved. The effectiveness of the proposed control scheme is evaluated and verified under various typical driving cycles.

1.3. Original Contributions

The main contributions of this paper include:

1. A nonlinear multi-objective model predictive control framework is developed for a FRIDEV under car-following scenarios, in which safety, car-following performance, ride comfort and energy economy are optimized simultaneously;
2. The demand power of the host vehicle is used as an indicator to accurately reflect the energy consumption and incorporated in the cost function to achieve enhanced energy economy.

1.4. Outline of the Paper

The rest of the paper is organized as follows. System modeling (vehicle longitudinal dynamics and electric drive system) is introduced in Section 2. Details of the proposed EOCFC strategy are elaborated in Section 3. The verification results under different driving cycles are discussed in Section 4. Conclusions and future work are given in Section 5.

2. System Modeling

2.1. Vehicle Longitudinal Dynamics

To tackle this multi-objective optimization problem, a state equation for the ACC system must be first established. In this study, the constant time headway (CTH) was employed as the desired inter-vehicle distance; so, the longitudinal kinematics of the preceding vehicle and the host vehicle, as shown in Figure 1, are expressed by:

$$\begin{cases} \Delta d = d - d_{\text{des}} \\ \Delta v = v_{\text{p}} - v_{\text{h}} \\ d_{\text{des}} = th \cdot v_{\text{h}} + d_0 \end{cases}, \tag{1}$$

where Δd is the spacing error; d denotes the actual inter-vehicle spacing; d_{des} represents the desired inter-vehicle spacing; th is the time headway; v_{h} represents the speed of the host vehicle; d_0 is the minimum allowable distance between the preceding vehicle and the host vehicle when both vehicles come to a complete stop; Δv is the speed error (i.e., the relative speed); and v_{p} denotes the speed of the preceding vehicle.

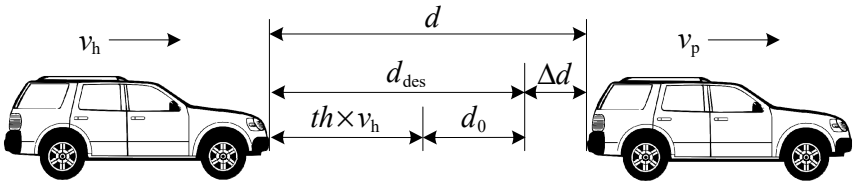

Figure 1. Longitudinal kinematics of the preceding vehicle and the host vehicle.

Taking the derivative of both sides of the above equations leads to:

$$\begin{cases} \Delta \dot{d} = \Delta v - th \times a_{\text{h}} \\ \Delta \dot{v} = a_{\text{p}} - a_{\text{h}} \end{cases}, \tag{2}$$

where a_{p} denotes the acceleration of the preceding vehicle, and a_{h} represents the acceleration of the host vehicle. Considering the response characteristics of the vehicle driving and braking systems, the acceleration of the host vehicle a_{h} can be modelled as a first-order system, as follows:

$$a_{\text{h}} = \frac{K_{\text{s}}}{T_0 s + 1} a_{\text{des}}, \tag{3}$$

where K_{s} denotes the DC gain of the system; T_0 represents the time constant of the system; and a_{des} stands for the desired acceleration.

Based on Equations (1)–(3), the following governing equations for the longitudinal inter-vehicle dynamics can be established:

$$\begin{cases} \dot{x} = A_0 x + B_0 u + G_0 w \\ y = C_0 x \end{cases}, \tag{4}$$

with

$$x = [\Delta d,\ \Delta v,\ a_{\text{h}}]^T,\ u = a_{\text{des}},\ w = a_{\text{p}}$$

$$A_0 = \begin{bmatrix} 0 & 1 & -th \\ 0 & 0 & -1 \\ 0 & 0 & -1/T_0 \end{bmatrix},\ B_0 = \begin{bmatrix} 0 \\ 0 \\ K_{\text{s}}/T_0 \end{bmatrix},\ G_0 = \begin{bmatrix} 0 \\ 1 \\ 0 \end{bmatrix},\ C_0 = \begin{bmatrix} 1 & 0 & 0 \\ 0 & 1 & 0 \\ 0 & 0 & 1 \end{bmatrix}$$

By means of zero-order hold, the above governing Equation (4) can be discretized as follows:

$$\begin{cases} x(k+1) = Ax(k) + Bu(k) + Gw(k) \\ y(k) = Cx(k) \end{cases}, \tag{5}$$

with

$$A = \sum_{k=0}^{\infty} \frac{{A_0}^k {T_s}^k}{k!},\ B = \sum_{k=0}^{\infty} \frac{{A_0}^{k-1} {T_s}^k}{k!} B_0,\ G = \sum_{k=0}^{\infty} \frac{{A_0}^{k-1} {T_s}^k}{k!} G_0,\ C = \begin{bmatrix} 1 & 0 & 0 \\ 0 & 1 & 0 \\ 0 & 0 & 1 \end{bmatrix}$$

where k denotes the time index, and T_s represents the sampling time.

Additionally, the longitudinal force equilibrium equation for the host vehicle can be characterized as follows:

$$\begin{aligned} T_d &= \left(mgf\cos\alpha + mg\sin\alpha + \frac{C_D A}{21.15} v^2 + \delta m \frac{dv}{dt} \right) \cdot r \\ &= (T_{m\_f} \times \eta_f + T_{m\_r} \times \eta_r) i_0 \end{aligned} \tag{6}$$

where T_d denotes the demand torque of vehicle; T_{m_f} and T_{m_r} represent the front and rear motor output torques; η_f and η_r are the front and rear reducer efficiencies; i_0 denotes the speed ratio of the front and rear reducers; r represents the tire radius; m is the vehicle curb mass; g is the gravitational acceleration; f denotes the rolling resistance coefficient; α stands for the road slope; C_D is the drag coefficient; A represents the frontal area; v is the vehicle longitudinal speed; and δ is the rotational mass coefficient.

2.2. Electric Drive System

As mentioned above, a FRIDEV is considered in this study. The layout of the electric drive system is shown in Figure 2. This powertrain is composed of two permanent-magnet synchronous motors (PMSMs), each of which is connected to two driving wheels via a reducer and a differential. These two motors are not mechanically connected to each other, so they can be independently controlled by their motor control units (MCUs). The battery provides power to the two PMSMs when driving and receives energy during regenerative braking, supervised by an onboard battery management system (BMS). The vehicle control unit serves as a control center for the entire powertrain, which receives signals from and sends control commands to the BMS and MCUs.

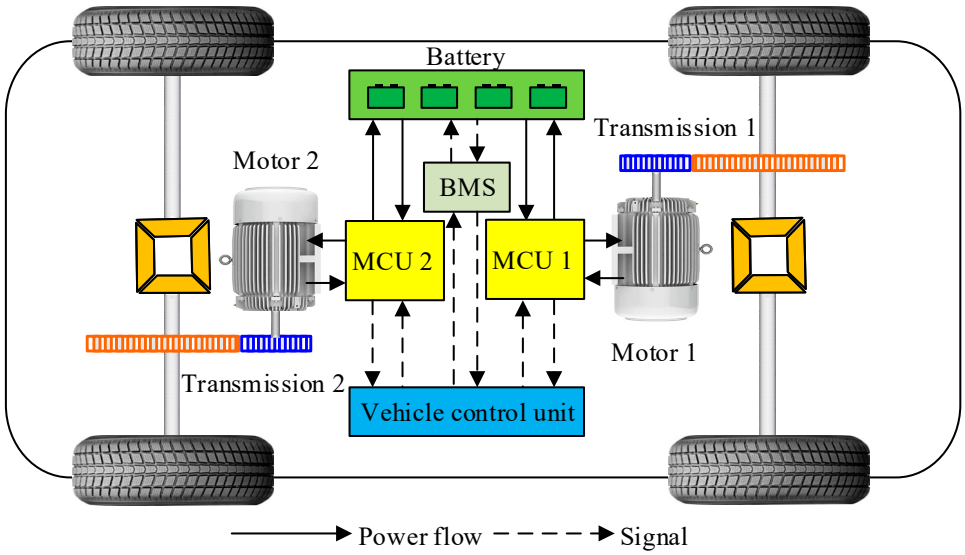

Figure 2. Layout of electric drive system.

The rotational speeds of the front and rear motors are governed by the following equation:

$$n_{m\_f} = n_{m\_r} = \frac{60 v i_0}{2\pi r} v i_0, \tag{7}$$

where n_{m_f} and n_{m_r} denote the rotational speeds of the front and rear motors on the host vehicle.

The total input power P_{m_in} of the two motors can be expressed as follows:

$$P_{m\_in} = \frac{T_{m\_f} n_{m\_f} + T_{m\_r} n_{m\_r}}{9550}, \tag{8}$$

Two motor efficiency maps, as shown in Figure 3, were used in this study to characterize the efficiencies of these two PMSMs under different operating conditions (i.e., different combinations of speeds and torques). Note that the maximum torque, maximum power and efficiency characteristics of these two PMSMs are different, which necessitates torque distribution between these two motors for economy optimization purposes.

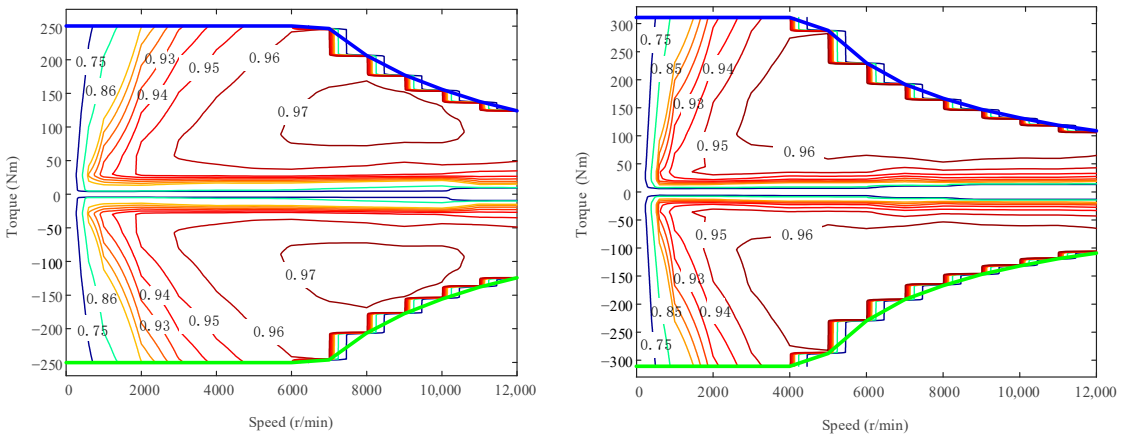

(**a**) (**b**)

Figure 3. Efficiency maps of front motor (**a**) and rear motor (**b**).

As for the battery system, a straightforward Rint battery model [22] was employed in this study, and the schematic of this model is shown in Figure 4. In this model, the battery is represented by an equivalent circuit containing a power source and a resistor.

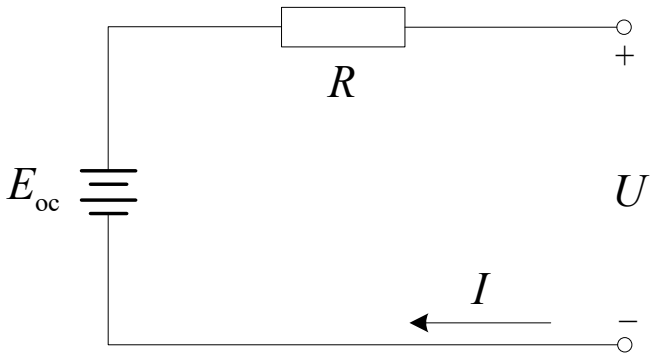

Figure 4. Schematic of Rint battery model.

Based on this Rint battery model, the battery output power can be written as:

$$P_b = UI, \tag{9}$$

where P_b denotes the battery output power; U represents the terminal voltage; and I is the charge or discharge current. The terminal voltage can be further expressed as:

$$U = E_{oc} - IR, \tag{10}$$

where E_{oc} represents the electromotive force, and R stands for the internal resistance.

Combining Equations (9) and (10) leads to:

$$I = \frac{E_{oc} - \sqrt{{E_{oc}}^2 - 4 \times R \times P_b}}{2 \times R}, \tag{11}$$

In this study, the battery state of charge (SOC) was calculated using the ampere-hour integral method, as follows:

$$SOC = SOC_0 - \frac{1}{C}\int_{t_1}^{t_2} \eta_b I \, dt, \tag{12}$$

where SOC_0 denotes the battery initial SOC; C represents the battery rated capacity; t_1 and t_2 are the starting and ending time for charging (or discharging); and η_b stands for the battery charging (or discharging) efficiency. The battery efficiency map used in this study is shown in Figure 5.

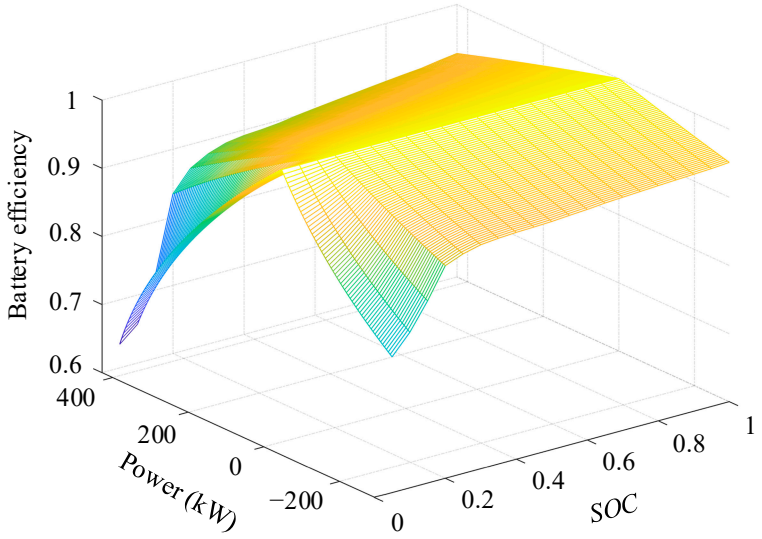

Figure 5. Battery efficiency map.

3. Economy-Oriented Car-Following Control Strategy

In the car-following mode, the host vehicle follows the preceding vehicle and maintains a safe inter-vehicle spacing. It is a challenging task to optimize the economy performance in this mode. On the one hand, the reduction in energy consumption can result in deterioration of car-following performance (i.e., increased spacing error). On the other hand, if the host vehicle strictly follows a desired inter-vehicle spacing, then its energy consumption is deterministic, and economy optimization becomes impossible. Hence, an appropriate trade-off between economy performance and car-following performance should be made. In this paper, the car-following requirement is properly relaxed without jeopardizing vehicle safety, and inter-vehicle spacing is maintained within a safe range. By this means, economy optimization in the car-following mode becomes achievable, as different inter-vehicle spacing can lead to different energy consumption. Indeed, the economy optimization task can be formulated as a multi-objective optimization problem, as shown in Figure 6.

3.1. Control Objectives

This section introduces the performance requirements that the ACC system needs to satisfy. The performance requirements should be properly determined, so that (1) the car-following performance, ride comfort and energy consumption are accurately quantified, and (2) the cost function appropriately reflects the interactions between the above performances. In this section, the above three types of performances are individually analyzed, followed by the design of a cost function which incorporates these performances.

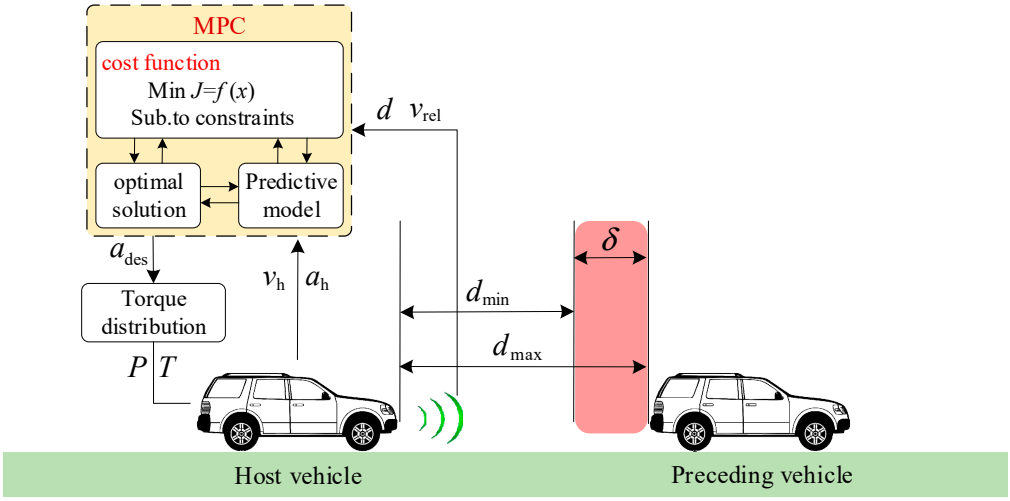

Figure 6. Schematic of the proposed EOCFC strategy.

A. Car-following performance

The car-following performance of an ACC system is normally evaluated by means of two indicators—spacing error and speed error (i.e., relative speed). Using these indicators, in this study, three important requirements were taken into consideration in quantifying the car-following performance. Firstly, the desired inter-vehicle spacing is strictly restrained within the allowable range (i.e., the green area in Figure 7). Secondly, both spacing error and speed error are maintained within a small range. Lastly, strict safety constraint is imposed on the actual inter-vehicle spacing.

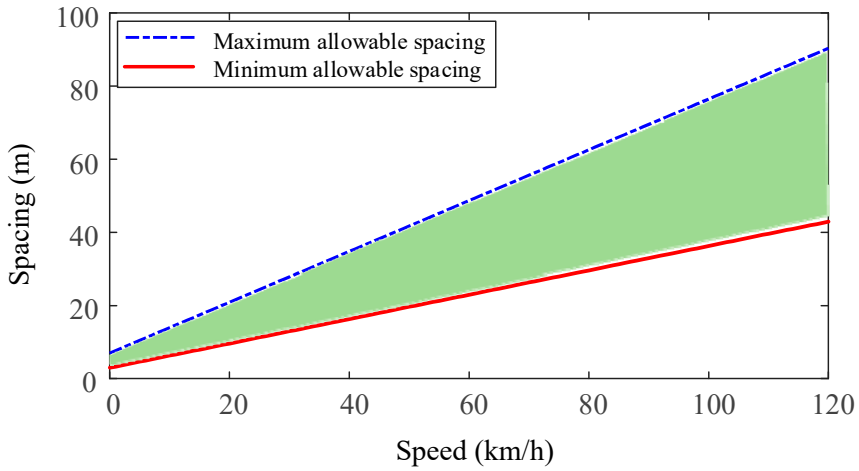

Figure 7. Longitudinal car-following distance.

For the first requirement, as shown in Figure 7, the upper and lower boundaries of the desired inter-vehicle spacing d_{des} can be written as:

$$d_{max} = th_{\max} \times v_{\mathrm{h}} + d_{0\_\max}, \quad (13)$$

$$d_{min} = th_{\min} \times v_{\mathrm{h}} + d_{0\_\min}, \quad (14)$$

where $d_{\max}$ and $d_{\min}$ are the maximum and minimum values of d_{des}; $th_{\max}$ and $th_{\min}$ denote the maximum and minimum values of th; and $d_{0\_\max}$ and $d_{0\_\min}$ represent the maximum and minimum values of d_0. In this study, $th_{\max}$ and $th_{\min}$ were chosen as 2.5 s and 1.2 s, respectively, while $d_{0\_\max}$ and $d_{0\_\min}$ are chosen as 3 m and 6 m, respectively. Note, that the desired inter-vehicle spacing d_{des} must fall between these two boundaries, i.e., it must fall within the green area shown in Figure 7.

For the second requirement, the spacing error Δd and the speed error Δv are constrained according to the following inequalities:

$$\Delta d_{\min} \leq \Delta d \leq \Delta d_{\max}, \tag{15}$$

$$\Delta v_{\min} \leq \Delta v \leq \Delta v_{\max}, \tag{16}$$

where $\Delta d_{\min} = d_{\min} - d_{\text{des}}$; $\Delta d_{\max} = d_{\max} - d_{\text{des}}$; and $\Delta v_{\max}$ and $\Delta v_{\min}$ are the upper and lower boundaries of Δv.

For the third requirement, to guarantee safety during ACC operation, the following constraint is imposed on the actual inter-vehicle spacing [23]:

$$d \geq \max\{TTC \cdot \Delta v, d_{\text{s}}\}, \tag{17}$$

where TTC denotes the time to collision, and d_{s} represents a fixed safe distance.

As mentioned above, car-following performance can be evaluated by means of spacing error and speed error (i.e., relative speed). Given that the above requirements (i.e., Equations (15)–(17)) are met, the car-following performance can be quantified as follows:

$$J_1 = \sigma_{\Delta d} \Delta d^2 + \sigma_{\Delta v} \Delta v^2, \tag{18}$$

where J_1 is the performance index quantifying the car-following performance, and coefficients $\sigma_{\Delta d}$ and $\sigma_{\Delta v}$ are the weighting factors for these two terms.

B. Ride comfort

Usually, acceleration and its time derivative (i.e., jerk) are employed to evaluate ride comfort of an ACC system [24]. To ensure ride comfort during ACC operation, the magnitudes of both acceleration and jerk should be properly constrained.

In this paper, the desired acceleration, desired jerk and actual acceleration of the host vehicle are employed to quantify ride comfort during ACC operation. Namely, the following performance index for ride comfort is defined:

$$J_2 = \sigma_{a1} a_{\text{des}}^2 + \sigma_{a2} \dot{a}_{\text{des}}^2 + \sigma_{a3} a_{\text{h}}^2, \tag{19}$$

where a_{des}, $\dot{a}_{\text{des}}$, and a_{h} denote the desired acceleration, desired jerk and actual acceleration of the host vehicle, respectively, and σ_{a1}, σ_{a2}, and σ_{a3} are the weighting factors for these three terms.

Additionally, the above-mentioned desired acceleration, desired jerk and actual acceleration are constrained as follows:

$$\begin{cases} a_{\min} \leq a_{\text{des}} \leq a_{\max} \\ j_{\min} \leq \dot{a}_{\text{des}} \leq j_{\max} \\ a_{\min} \leq a_{\text{h}} \leq a_{\max} \end{cases}, \tag{20}$$

where $a_{\max}$ and $a_{\min}$ are the upper and lower boundaries for acceleration, while $j_{\max}$ and $j_{\min}$ denote the upper and lower boundaries for jerk.

C. Energy consumption

In the existing literature, energy consumption during ACC operation is mainly quantified in three different ways: (a) energy consumption is represented by the 2-norm of acceleration and the 2-norm of jerk [15], (b) energy consumption is quantified using the 2-norm of acceleration error [17], and (c) energy consumption is approximated as a convex function of acceleration and speed [20].

Note that in the above approaches the energy consumption is not directly quantified as the product of power and time; instead, it is indirectly represented as a function of energy-related quantities, such as acceleration and speed. The underlying reason is that by doing so, the computation difficulties caused by nonlinearities in the subsequent receding-horizon optimization stage can be avoided. However, the above representations of energy consumption are only reasonable approximations, and errors are inevitably present in these forms of approximate representations. Considering this limitation, in this paper, a more direct and accurate representation of energy consumption is employed. Specifically, by definition, the energy consumed during ACC operation is the integral of power over time, as follows:

$$J_3 = \sigma_{\mathrm{p}} \int P \mathrm{d}t = \sigma_{\mathrm{p}} \int \frac{Tn}{9550} \mathrm{d}t, \tag{21}$$

where J_3 denotes the economy performance index; σ_{p} represents the weighting factor for this performance; P is the output power of the powertrain; T is the output torque of the powertrain; and n is the rotational speed of motor. Note that T and n can be further expressed as follows:

$$\frac{Ti_0}{r} = mgf\cos\alpha + mg\sin\alpha + \frac{C_{\mathrm{D}}A}{21.15}v_{\mathrm{h}}^2 + \delta m a_{\mathrm{des}}, \tag{22}$$

$$n = \frac{v_{\mathrm{h}} i_0}{0.377r}, \tag{23}$$

It should be emphasized that Equation (21)—the integral of power over time—is the most precise representation of energy consumption during ACC operation. By this means, the errors existing in the current forms of energy consumption representations are eliminated, which in turn improves the economy performance of ACC systems. This is also the major innovation and contribution of this paper.

3.2. Overall Cost Function

Combining the above three performance indices for car-following performance, ride comfort and energy consumption, the overall performance index (i.e., cost function) for the ACC car-following mode is obtained:

$$\begin{aligned} J_0 &= J_1 + J_2 + J_3 \\ &= \sigma_{\Delta d}\Delta d^2 + \sigma_{\Delta v}\Delta v^2 + \sigma_{a1}a_{\mathrm{des}}^2 + \sigma_{a2}\dot{a}_{\mathrm{des}}^2 + \sigma_{a3}a_{\mathrm{h}}^2 + \sigma_{\mathrm{p}}\int P\mathrm{d}t \end{aligned} \tag{24}$$

Equation (24) can be further formatted as follows:

$$J_0 = y^T \sigma_y y + \sigma_{a1}u^2 + \sigma_{a2}\dot{u}^2 + \sigma_{\mathrm{p}}\int P dt, \tag{25}$$

with

$$y = [\Delta d,\ \Delta v,\ a_{\mathrm{h}}]^T,\ \sigma_y = \begin{bmatrix} \sigma_{\Delta d} & 0 & 0 \\ 0 & \sigma_{\Delta v} & 0 \\ 0 & 0 & \sigma_{a3} \end{bmatrix}$$

Additionally, based on Equations (15)–(17) and (20), the corresponding constraints for the above cost function are rewritten as:

$$\begin{bmatrix} \Delta d_{\min} \\ \Delta v_{\min} \\ a_{\min} \end{bmatrix} \le y \le \begin{bmatrix} \Delta d_{\max} \\ \Delta v_{\max} \\ a_{\max} \end{bmatrix}, \tag{26}$$

$$\begin{bmatrix} 1 & -TTC - th \\ 1 & -th \end{bmatrix} \begin{bmatrix} \Delta d \\ \Delta v \end{bmatrix} \ge \begin{bmatrix} -th \cdot v_{\mathrm{p}} - d_0 \\ -th \cdot v_{\mathrm{p}} - d_0 + d_{\mathrm{s}} \end{bmatrix}, \tag{27}$$

$$\begin{cases} a_{\min} \le u \le a_{\max} \\ j_{\min} \le \dot{u} \le j_{\max} \end{cases}, \tag{28}$$

3.3. Model Predictive Optimization Problem

To reduce energy consumption while satisfying car-following performance and ride comfort, in this work, a multi-objective optimization problem was established for ACC systems under the framework of model predictive control (MPC). The process of constructing this optimization problem is explained below.

Based on Equation (5), the predicted system state can be written as:

$$\begin{cases} X(k+N_{\mathrm{P}}|k) = \tilde{A}x(k) + \widetilde{B}U(k+N_{\mathrm{C}}) + \widetilde{G}W(k+N_{\mathrm{P}}) \\ Y(k+N_{\mathrm{P}}|k) = \widetilde{D}x(k) + \widetilde{E}U(k+N_{\mathrm{C}}) + \widetilde{F}W(k+N_{\mathrm{P}}) \end{cases}, \tag{29}$$

where N_{P} denotes the prediction horizon; N_{C} represents the control horizon; and matrices X, Y, U, W, $\widetilde{A}$, $\widetilde{B}$, $\widetilde{G}$, $\widetilde{D}$, $\widetilde{E}$, $\widetilde{F}$ are given by:

$$X(k+N_{\mathrm{P}}|k)=\begin{bmatrix} x(k+1|k) \\ x(k+2|k) \\ \vdots \\ x(k+N_{\mathrm{P}}|k) \end{bmatrix},\ Y(k+N_{\mathrm{P}}|k)=\begin{bmatrix} y(k+1|k) \\ y(k+2|k) \\ \vdots \\ y(k+N_{\mathrm{P}}|k) \end{bmatrix}$$

$$U(k+N_{\mathrm{C}})=\begin{bmatrix} u(k) \\ u(k+1) \\ \vdots \\ u(k+N_{\mathrm{C}}-1) \end{bmatrix},\ W(k+N_{\mathrm{P}})=\begin{bmatrix} w(k) \\ w(k+1) \\ \vdots \\ w(k+N_{\mathrm{P}}-1) \end{bmatrix}$$

$$\widetilde{A}=\begin{bmatrix} A \\ A^2 \\ \vdots \\ A^{N_{\mathrm{P}}} \end{bmatrix},\ \widetilde{B}=\begin{bmatrix} B & 0 & \cdots & 0 \\ AB & B & \cdots & \vdots \\ \vdots & \vdots & \ddots & 0 \\ A^{N_{\mathrm{P}}-1}B & A^{N_{\mathrm{P}}-2}B & \cdots & A^{N_{\mathrm{P}}-N_{\mathrm{C}}}B \end{bmatrix}$$

$$\widetilde{G}=\begin{bmatrix} G & 0 & \cdots & 0 \\ AG & G & \cdots & \vdots \\ \vdots & \vdots & \ddots & 0 \\ A^{N_{\mathrm{P}}-1}G & A^{N_{\mathrm{P}}-2}G & \cdots & A^{N_{\mathrm{P}}-N_{\mathrm{C}}}G \end{bmatrix}$$

$$\widetilde{D}=\begin{bmatrix} CA \\ CA^2 \\ \vdots \\ CA^{N_{\mathrm{P}}} \end{bmatrix},\ \widetilde{E}=\begin{bmatrix} CB & 0 & \cdots & 0 \\ CAB & CB & \cdots & \vdots \\ \vdots & \vdots & \ddots & 0 \\ CA^{N_{\mathrm{P}}-1}B & CA^{N_{\mathrm{P}}-2}B & \cdots & CA^{N_{\mathrm{P}}-N_{\mathrm{C}}}B \end{bmatrix}$$

$$\widetilde{F}=\begin{bmatrix} CG & 0 & \cdots & 0 \\ CAG & CG & \cdots & \vdots \\ \vdots & \vdots & \ddots & 0 \\ CA^{N_{\mathrm{P}}-1}G & CA^{N_{\mathrm{P}}-2}G & \cdots & CA^{N_{\mathrm{P}}-N_{\mathrm{C}}}G \end{bmatrix}$$

The original cost function in continuous time domain is given by Equation (25). To construct the optimization problem, this cost function is first discretized and then extended to the entire prediction horizon, as follows:

$$\begin{aligned} J(y,u,\Delta u,P) &= \sum_{i=0}^{N_{\mathrm{P}}-1}\|y(k+i+1|k)\|^2_{\sigma_y}+\sum_{i=0}^{N_{\mathrm{P}}-1}\|u(k+i|k)\|^2_{\sigma_u} \\ &+\sum_{i=0}^{N_{\mathrm{P}}-1}\|\Delta u(k+i|k)\|^2_{\sigma_{\Delta u}} \\ &+\sum_{i=0}^{N_{\mathrm{P}}-1}\left\{\sigma_{\mathrm{p}}P(k+i+1\big|k)T_{\mathrm{s}}\right\} \end{aligned} \tag{30}$$

where $J(y,u,\Delta u,P)$ represents the cost function for the entire prediction horizon; $\|\cdot\|^2_{\sigma}$ denotes the weighted 2-norm; and σ_y, σ_u, $\sigma_{\Delta u}$ and σ_{p} are the weighting factors.

Based on Equations (26)–(28), the constraints for the above cost function can be rewritten in the following form:

$$\begin{bmatrix} \Delta d_{\min} \\ \Delta v_{\min} \\ a_{\min} \end{bmatrix} \le y(k+i+1|k) \le \begin{bmatrix} \Delta d_{\max} \\ \Delta v_{\max} \\ a_{\max} \end{bmatrix},\ i=0:N_{\mathrm{P}}-1, \tag{31}$$

$$\begin{bmatrix} 1 & -TTC-th & 0 \\ 1 & -th & 0 \\ 0 & 0 & 0 \end{bmatrix}\cdot y(k+i+1|k) \ge \begin{bmatrix} -th \\ -th \\ 0 \end{bmatrix} v_{\mathrm{p}}(k+i+1|k)+\begin{bmatrix} -d_0 \\ -d_0+d_{\mathrm{s}} \\ 0 \end{bmatrix},\ i=0:N_{\mathrm{P}}-1, \tag{32}$$

$$\begin{cases} a_{\min} \le u(k+i|k) \le a_{\max} \\ j_{\min} \cdot T_s \le \Delta u(k+i|k) \le j_{\max} \cdot T_s \end{cases}, \; i = 0 : N_P - 1, \tag{33}$$

Based on the above derivations for system state, cost function and constraints, the multi-objective optimization problem for economy-oriented ACC systems can be established as follows:

$$\begin{aligned} \min_{u(k+i|k), i=0:N_P-1} J(y, u, \Delta u, P) \quad &= \sum_{i=0}^{N_P-1} \|y(k+i+1|k)\|^2_{\sigma_y} + \sum_{i=0}^{N_P-1} \|u(k+i|k)\|^2_{\sigma_u} \\ &+ \sum_{i=0}^{N_P-1} \|\Delta u(k+i|k)\|^2_{\sigma_{\Delta u}} \\ &+ \sum_{i=0}^{N_P-1} \left\{\sigma_p P(k+i+1|k) T_s\right\} \end{aligned} \tag{34}$$

Subj. to:

1. The discrete system state Equation (5);
2. The constraints (31)–(33).

Note that Equation (34) is a nonlinear optimization problem, as the energy consumption index is a nonlinear function of the host vehicle's acceleration and speed. To find a solution to this problem, in this study, an S-Function was devised in MATLAB by means of exhaustive search. Note that the exhaustive search method has also been employed in relevant work in the literature, such as [5,25], to tackle similar optimization problems. Interested readers are referred to [5,25] for more details.

4. Simulation Results

To verify the effectiveness of the proposed EOCFC strategy in car-following scenarios, a complete simulation environment, including a preceding vehicle and a host vehicle, was established using CarSim and MATLAB/Simulink in this study. In the simulation studies, the preceding vehicle is controlled to track the speed profile of NEDC, UDDS and WLTC test cycles, and the host vehicle follows the preceding vehicle using either the proposed EOCFC strategy or its competing method—multi-objective ACC (MO-ACC) [15]. It should be mentioned that for both EOCFC and MO-ACC, the optimal torque distribution strategy proposed in [26] is used to determine the torques of the front and rear motors. Since torque distribution is not a focus of this paper, it is not further discussed in the following text. The simulation parameters used are listed in Table 1.

4.1. Car-Following and Ride Comfort Performance

Figures 8 and 9 demonstrate the host vehicle speed profile and the inter-vehicle spacing resulting from the MO-ACC strategy and the EOCFC strategy, under the typical WLTC test cycle. In terms of vehicle speed, these competing strategies perform similarly, and both closely track the speed profile of the WLTC test cycle. However, these two algorithms provide very different spacing patterns: the MO-ACC strictly follows the desired inter-vehicle spacing, while the EOCFC yields an inter-vehicle spacing located within the upper and lower spacing boundaries, as explained in Section 3.1. This difference indicates that with the proposed EOCFC strategy onboard, the requirement on car-following performance is relaxed without jeopardizing vehicle safety (namely, the actual inter-vehicle spacing is maintained within a safe range). By this means, optimization of ACC economy performance in the car-following scenario can be made possible.

The acceleration results of the host vehicle using these two competing strategies are plotted in Figure 10. It is seen that under the WLTC test cycle, the acceleration amplitude resulting from EOCFC is smaller than the amplitude produced by MO-ACC, indicating that the proposed EOCFC provides superior ride comfort. The underlying reason for this superiority is that the demand power of the host vehicle is incorporated in the cost function, which reduces the occurrence of high-power operation of the host vehicle.

Table 1. Simulation parameters.

Parameters	Unit	Value
m	kg	2270
A	m^2	3.0
C_D	-	0.3
f	-	0.008
r	m	0.393
i_0	-	10.885
α	deg	0
th	s	1.5
th_{min}	s	1.2
th_{max}	s	2.5
d_0	m	5
d_{0_min}	m	3
d_{0_max}	m	6
Δv_{min}	m/s	−3.5
Δv_{max}	m/s	4
TTC	s	−2.5
d_s	m	3
a_{min}	m/s^2	−2.8
a_{max}	m/s^2	1.2
j_{min}	m/s^3	−6
j_{max}	m/s^3	6

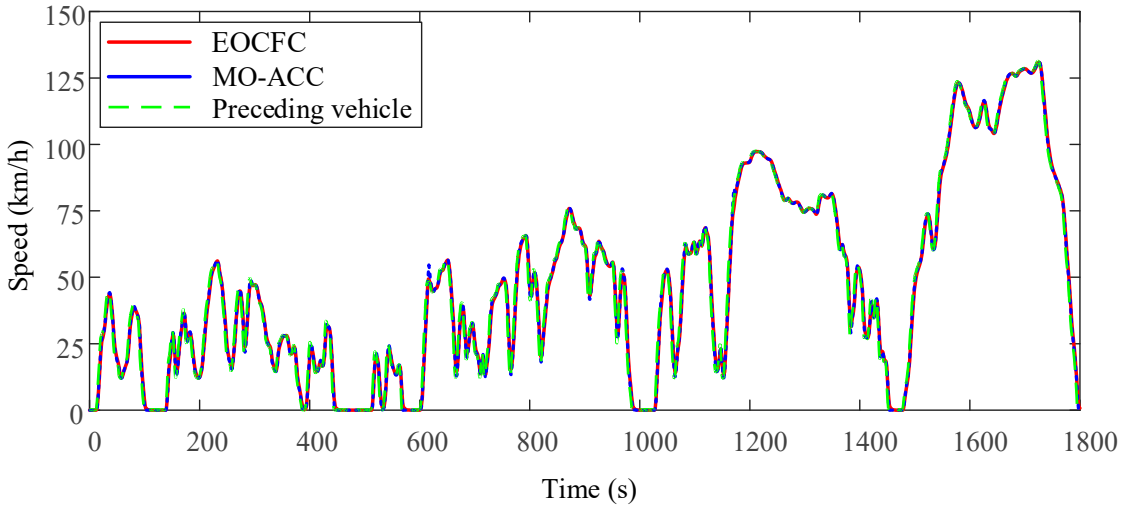

Figure 8. Speed profile of the host vehicle resulting from the MO-ACC strategy and the EOCFC strategy under the WLTC test cycle.

4.2. Energy Economy

The energy consumption resulting from these two algorithms under three standard test cycles are given in Table 2. It is seen that EOCFC outperforms MO-ACC for all three test cycles; specifically, EOCFC reduces energy consumption by 0.53%, 3.33% and 1.51% under NEDC, UDDS and WLTC test cycles, respectively.

Table 2. Energy consumption under various test cycles (initial SOC = 0.8).

Control Scheme	Energy Consumption (kWh)		
	NEDC	UDDS	WLTC
MO-ACC	1.3687	1.3762	3.5537
EOCFC	1.3614	1.3304	3.5000
Improvement	0.53%	3.33%	1.51%

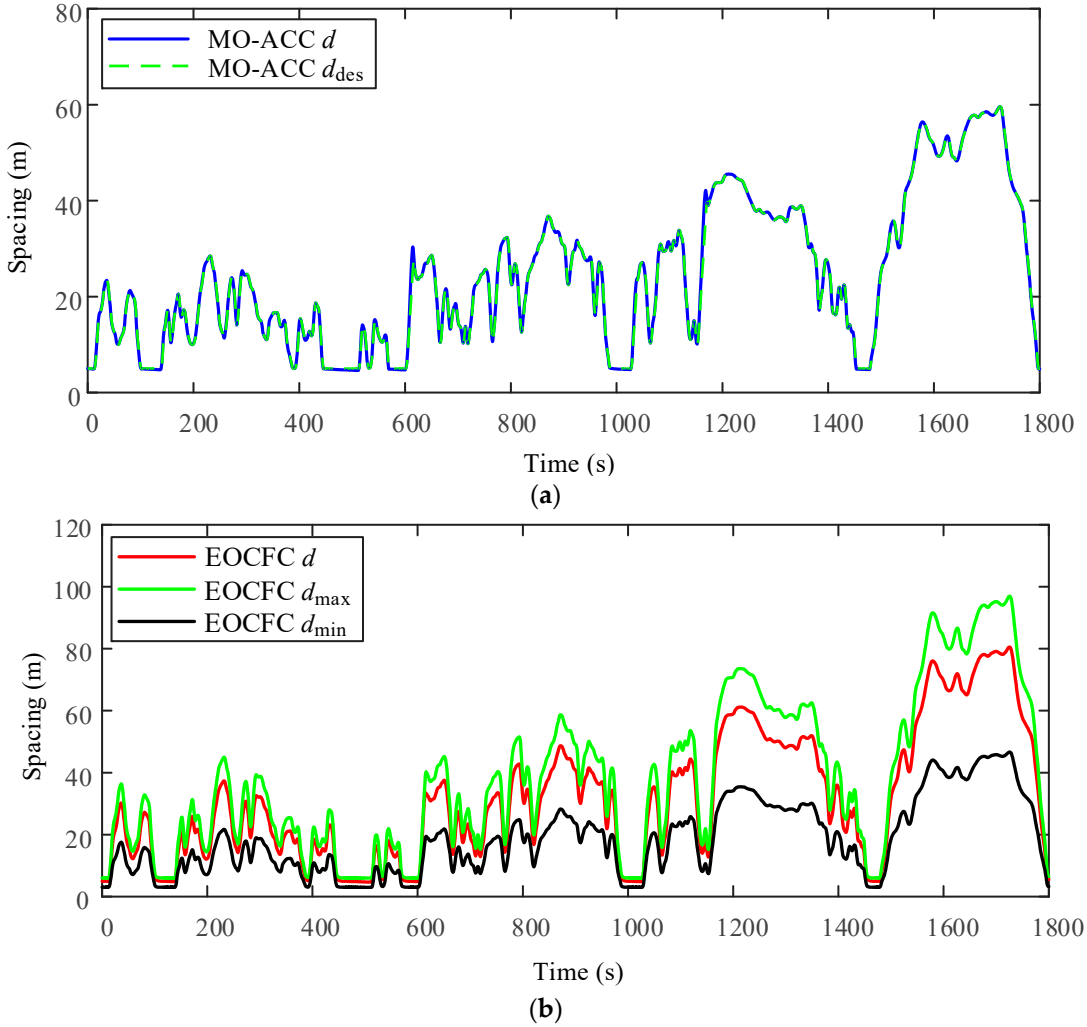

Figure 9. Inter-vehicle spacing resulting from the MO-ACC strategy (**a**) and the EOCFC strategy (**b**) under the WLTC test cycle.

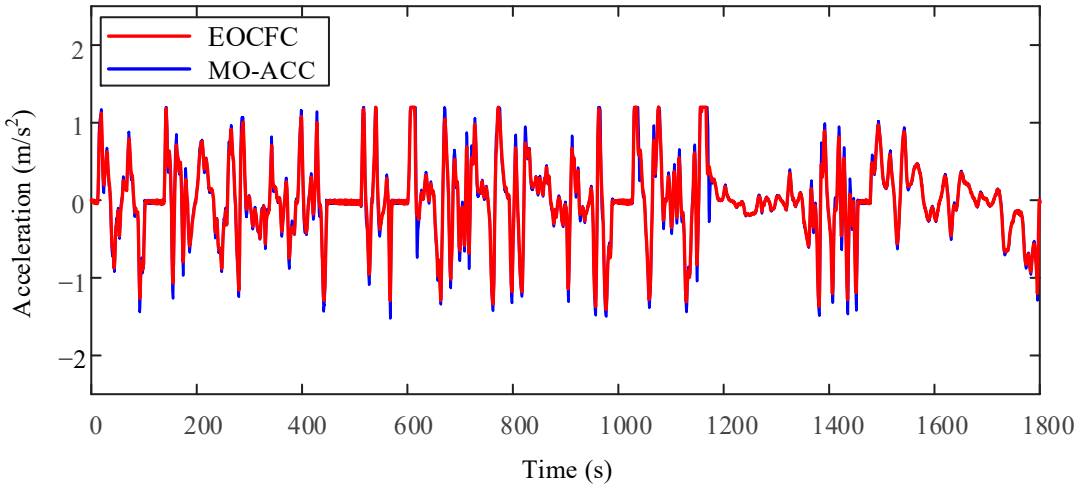

Figure 10. Acceleration of the host vehicle using MO-ACC and EOCFC under the WLTC test cycle.

It should be noted that the above percentages may seem like small numbers, but considering the large number of existing electric vehicles in the world and especially their quickly-growing sales, a small percentage of energy economy improvement can bring about magnificent economic benefits in total. Therefore, the 0.53%~3.33% energy

saving ratio reported in this paper is not negligible but indeed significant. Moreover, as mentioned in Section 3, this study is dealing with a multi-objective optimization problem in which three types of performance (i.e., car-following performance, ride comfort and energy consumption) should be simultaneously taken into consideration. In other words, when optimizing energy economy, we need to make sure that the other two performances (car-following performance and ride comfort) do not seriously deteriorate. Hence, the final result we present in this article is an optimal outcome that achieves a good balance between these three performances.

5. Conclusions and Future Work

ACC has been widely considered as a promising approach to reduction in energy consumption of modern vehicles. In this paper, an EOCFC strategy is proposed to improve energy economy of a FRIDEV in car-following scenarios. The energy consumption of this vehicle is accurately quantified by means of its demand power, which is incorporated in the cost function for energy optimization. Without jeopardizing car-following performance and ride comfort, the energy economy in car-following scenarios is improved. The proposed EOCFC strategy is evaluated under the standard NEDC, UDDS and WLTC test cycles, in comparison with a benchmark method, MO-ACC. The results show that EOCFC decreases energy consumption by 1.3687 kWh, 1.3762 kWh and 3.5537 kWh under NEDC, UDDS and WLTC driving cycles, achieving economy improvements of 0.53%, 3.33% and 1.51%, respectively.

In our future studies, car-following control strategies for vehicle platoons will be investigated, and effects of road slope and traffic information will be taken into consideration in economy optimization of vehicle platoons.

Author Contributions: Conceptualization, Y.L. and C.F.; methodology, Y.L.; validation, C.G., C.Y. and Z.Y.; formal analysis, Y.L.; writing—original draft preparation, Y.L. and C.G.; writing—review and editing, C.Y. and C.F.; supervision, C.F.; project administration, Z.Y. and C.F.; funding acquisition, C.F. All authors have read and agreed to the published version of the manuscript.

Funding: This research was funded by the Natural Science Foundation of Chongqing under grant cstc2020jcyj-msxmX0664, and the Fundamental Research Funds for the Central Universities under grant 2020CDJ-LHZZ-043.

Data Availability Statement: The data presented in this study are embedded in the context of this paper.

Conflicts of Interest: The authors declare no conflict of interest. The funders had no role in the design of the study; in the collection, analyses, or interpretation of data; in the writing of the manuscript; or in the decision to publish the results. Zhong Yang is the employee of Chongqing Changan Automobile. The paper reflects the views of the scientists and not the company.

References

1. Rajashekara, K. Present status and future trends in electric vehicle propulsion technologies. *IEEE J. Emerg. Sel. Top. Power Electron.* **2013**, *1*, 3–10. [CrossRef]
2. Mutoh, N. Front-and-rear-wheel-independent-drive-type electric vehicle (FRID EV) with compatible driving performance and safety. *World Electr. Veh. J.* **2009**, *3*, 17–26. [CrossRef]
3. Barkenbus, J.N. Eco-driving: An overlooked climate change initiative. *Energy Policy* **2010**, *38*, 762–769. [CrossRef]
4. Kamal, M.; Mukai, M.; Murata, J.; Kawabe, T. Ecological driver assistance system using model-based anticipation of vehicle–road–traffic information. *IET Intell. Transp. Syst.* **2010**, *4*, 244–251. [CrossRef]
5. Guo, C.; Fu, C.; Luo, R.; Yang, G. Energy-oriented car-following control for a front-and rear-independent-drive electric vehicle platoon. *Energy* **2022**, *257*, 124732. [CrossRef]
6. Li, S.; Xu, S.; Wang, W.; Cheng, B. Overview of ecological driving technology and application for ground vehicles. *J. Automot. Saf. Energy* **2014**, *5*, 121–131.
7. Beusen, B.; Broekx, S.; Denys, T.; Beckx, C.; Degraeuwe, B.; Gijsbers, M.; Scheepers, K.; Govaerts, L.; Torfs, R.; Panis, L.I. Using on-board logging devices to study the longer-term impact of an eco-driving course. *Transp. Res. Part D Transp. Environ.* **2009**, *14*, 514–520. [CrossRef]
8. Gilbert, E.G. Vehicle cruise: Improved fuel economy by periodic control. *Automatica* **1976**, *12*, 159–166. [CrossRef]

9. Chen, X.; Yang, J.; Zhai, C.; Lou, J.; Yan, C. Economic adaptive cruise control for electric vehicles based on ADHDP in a car-following scenario. *IEEE Access* **2021**, *9*, 74949–74958. [CrossRef]
10. Li, S.E.; Peng, H.; Li, K.; Wang, J. Minimum fuel control strategy in automated car-following scenarios. *IEEE Trans. Veh. Technol.* **2012**, *61*, 998–1007. [CrossRef]
11. Li, S.E.; Peng, H. Strategies to minimize the fuel consumption of passenger cars during car-following scenarios. *Proc. Inst. Mech. Eng. Part D J. Automob. Eng.* **2012**, *226*, 419–429. [CrossRef]
12. Ioannou, P.A.; Stefanovic, M. Evaluation of ACC vehicles in mixed traffic: Lane change effects and sensitivity analysis. *IEEE Trans. Intell. Transp. Syst.* **2005**, *6*, 79–89. [CrossRef]
13. Zhang, J.; Ioannou, P.A. Longitudinal control of heavy trucks in mixed traffic: Environmental and fuel economy considerations. *IEEE Trans. Intell. Transp. Syst.* **2006**, *7*, 92–104. [CrossRef]
14. Wu, C.; Zhao, G.; Ou, B. A fuel economy optimization system with applications in vehicles with human drivers and autonomous vehicles. *Transp. Res. Part D Transp. Environ.* **2011**, *16*, 515–524. [CrossRef]
15. Li, S.; Li, K.; Rajamani, R.; Wang, J. Model predictive multi-objective vehicular adaptive cruise control. *IEEE Trans. Control. Syst. Technol.* **2010**, *19*, 556–566. [CrossRef]
16. Eben Li, S.; Li, K.; Wang, J. Economy-oriented vehicle adaptive cruise control with coordinating multiple objectives function. *Veh. Syst. Dyn.* **2013**, *51*, 1–17. [CrossRef]
17. Luo, L.-h.; Liu, H.; Li, P.; Wang, H. Model predictive control for adaptive cruise control with multi-objectives: Comfort, fuel-economy, safety and car-following. *J. Zhejiang Univ. SCIENCE A* **2010**, *11*, 191–201. [CrossRef]
18. Schmied, R.; Waschl, H.; Del Re, L. Extension and experimental validation of fuel efficient predictive adaptive cruise control. In Proceedings of the 2015 American Control Conference (ACC), Chicago, IL, USA, 1–3 July 2015; pp. 4753–4758.
19. Jia, Y.; Jibrin, R.; Itoh, Y.; Görges, D. Energy-optimal adaptive cruise control for electric vehicles in both time and space domain based on model predictive control. *IFAC-PapersOnLine* **2019**, *52*, 13–20. [CrossRef]
20. Jia, Y.; Saito, T.; Itoh, Y.; Nukezhanov, Y.; Görges, D. Energy-optimal adaptive cruise control in time domain based on model predictive control. *IFAC-PapersOnLine* **2018**, *51*, 846–853. [CrossRef]
21. Madhusudhanan, A.K. A method to improve an electric vehicle's range: Efficient Cruise Control. *Eur. J. Control.* **2019**, *48*, 83–96. [CrossRef]
22. He, H.; Xiong, R.; Fan, J. Evaluation of lithium-ion battery equivalent circuit models for state of charge estimation by an experimental approach. *Energies* **2011**, *4*, 582–598. [CrossRef]
23. Moon, S.; Yi, K. Human driving data-based design of a vehicle adaptive cruise control algorithm. *Veh. Syst. Dyn.* **2008**, *46*, 661–690. [CrossRef]
24. Martinez, J.-J.; Canudas-de-Wit, C. A safe longitudinal control for adaptive cruise control and stop-and-go scenarios. *IEEE Trans. Control. Syst. Technol.* **2007**, *15*, 246–258. [CrossRef]
25. Li, L.; Wang, X.; Song, J. Fuel consumption optimization for smart hybrid electric vehicle during a car-following process. *Mech. Syst. Signal Process.* **2017**, *87*, 17–29. [CrossRef]
26. Cao, K.; Hu, M.; Wang, D.; Qiao, S.; Guo, C.; Fu, C.; Zhou, A. All-wheel-drive torque distribution strategy for electric vehicle optimal efficiency considering tire slip. *IEEE Access* **2021**, *9*, 25245–25257. [CrossRef]